
Article:
Hsia, F-C., Elam, F.M., Bonn, D. et al. (2020) Wear particle dynamics drive the difference between repeated and non-repeated reciprocated sliding. Tribology International, 142. 105983. ISSN: 0301-679X

https://doi.org/10.1016/j.triboint.2019.105983

Tribology International 142 (2020) 105983

Contents lists available at ScienceDirect

Tribology International

journal homepage: http://www.elsevier.com/locate/triboint

Wear particle dynamics drive the difference between repeated and non-repeated reciprocated sliding

Feng-Chun Hsia [a,b], Fiona M. Elam [a], Daniel Bonn [b], Bart Weber [a,b], Steve E. Franklin [a,c,d,*]

[a] Advanced Research Center for Nanolithography (ARCNL), Science Park 106, 1098XG, Amsterdam, the Netherlands
[b] Van der Waals-Zeeman Institute, IoP, University of Amsterdam, Science Park 904, 1098XH, Amsterdam, the Netherlands
[c] Department of Materials Science and Engineering, The University of Sheffield, Sheffield S1 3JD, UK
[d] ASML Research, De Run 6501, 5504DR, Veldhoven, the Netherlands

ARTICLE INFO

Keywords:
Friction
Wear
Adhesion
Third body

ABSTRACT

The dependence of the sliding mode (repeated vs. non-repeated reciprocated sliding) on the friction and wear behavior of ball-on-flat, brittle non-metallic interfaces in ambient air conditions is evaluated. Repeated sliding promotes the formation of a third body (compressed wear particles) that stabilizes the friction. Non-repeated sliding shows reduced evidence of third body formation, and instead a steady increase in friction. The proposed mechanism driving the non-repeated friction behavior is attributed to a gradual reduction in the ball surface roughness, leading to an increased area of real contact and greater capillary bridge forming across non-contact regions of the interface.

1. Introduction

Friction and wear are of paramount importance to the performance and lifetime of applications with high economic and societal impact such as engines, wheels and industrial production machines [1]. Estimates show that tribological contacts consume 23% of the world energy budget: 20% is spent on overcoming friction and 3% on repairing or substituting components that have worn as a result of friction [2]. These staggering numbers and the applications that they represent have motivated numerous experiments that aim to understand, manipulate and reduce friction and wear under industrially relevant conditions, mimicking for instance the behavior of combustion engines [3], turbines [4], train wheels [5], robotic grasping [6] and micro- and nano-electromechanical systems [7]. While some of these applications involve repeated, reciprocated sliding of the same two surfaces against each other, others slide in a non-repeated fashion, meaning that the slider always contacts a fresh, unworn counter surface. Examples of the latter include rolling wheels [8], walking [9], grabbing [10] (grabbing or clamping typically involves slip due to misalignment and curvature of the touching surfaces), cutting [11], read/write cycles of hard drives [12] and even atomic force microscopy imaging [13,14]. Interestingly, experiments that are designed to reproduce the frictional behavior observed in various applications are almost exclusively [15–17] performed in a repeated fashion [3,4,18] — also when the application involves non-repeated sliding [5,8,11,19]. Furthermore, the potential consequences this has for the tribological behavior is often overlooked. Here, we systematically study the friction and wear behavior of various types of nominally dry contacts between brittle non-metallic materials sliding in repeated or non-repeated fashion.

2. Experiment

In the ball-on-flat friction experiments (Fig. 1a inset), Al_2O_3 (sapphire), silicon carbide (SiC) and glass balls were slid against Si wafers or glass flats in repeated and non-repeated fashion in ambient air (21–23 °C, 20–60% relative humidity). These two different sliding modes are illustrated in the inset of Fig. 1a: in non-repeated sliding the ball was lifted after each forward and backward stroke (1 cycle), and placed back into contact with an untouched part of the flat. During repeated sliding the ball was reciprocated at a fixed location on the flat. In both the repeated and the non-repeated experiments, the stroke length (L), normal force (F_n) and sliding speed (v) were kept constant at 20 mm, 0.1 N and 0.5 mm/s, respectively. These materials and experimental parameters were chosen to resemble the silicon wafer-on-support contacts that limit the positioning accuracy in nano-lithography machines [20]. The used materials and their RMS roughness

* Corresponding author. Advanced Research Center for Nanolithography (ARCNL), Science Park 106, 1098XG, Amsterdam, the Netherlands.
E-mail address: s.franklin@arcnl.nl (S.E. Franklin).

https://doi.org/10.1016/j.triboint.2019.105983
Received 12 June 2019; Received in revised form 10 September 2019; Accepted 27 September 2019
Available online 30 September 2019

are further described in Table 1. The tribological experiments were carried out using a Universal Mechanical Tester (UMT TriboLab, Bruker) that was set to acquire force and position data at a rate of 5 Hz. Each friction experiment consisted of 150 cycles, totaling a sliding distance of 6 m. In the non-repeated experiments, the time required to move the ball between subsequent cycles was approximately 27 s.

To characterize the wear of the sliding bodies, optical focus variation profilometry measurements were performed ex-situ using a laser scanning confocal microscope (Keyence VK-X1000). Furthermore, the wear scars on the balls and the wear tracks on the Si flats were imaged and analyzed using scanning electron microscopy (SEM, FEI Verios 460) and SEM-integrated energy dispersive X-ray (EDX, Oxford) measurements. The surface topography of the sliding bodies was measured by tapping mode atomic force microscopy (AFM, Bruker Dimension Icon) where the nominal tip radius of AFM tips carried out in the measurements was 8 nm.

3. Results and discussion

Fig. 1a shows the evolution of the measured friction force (F_f) as a function of the sliding distance for the repeated and non-repeated sapphire-on-Si wafer experiments. In the repeated sapphire-on-Si wafer experiments strong fluctuations in friction were initially observed, followed by a more stable friction force of roughly 50 mN after the first ~0.2 m of sliding (see Fig. S1a). The non-repeated version of the otherwise identical experiment resulted, in the majority of cases, in clearly different frictional behavior: the initial friction fluctuations observed during repeated sliding were not present and the friction force increased gradually with sliding distance. After 6 m of sliding the friction force had doubled, from ~55 mN to ~110 mN. It should be noted that this behavior was not observed in all experiments; in a few cases we observed run-in behavior followed by a stable friction force, see Fig. S2. This is discussed later in relation to third body formation. In the SiC-on-Si wafer experiments (Fig. 1b), the frictional behavior is qualitatively similar to that observed in the sapphire-on-Si wafer experiments. In the repeated SiC-on-Si wafer experiment, unstable friction run-in behavior during the first ~0.4 m of sliding is followed by a more stable evolution of the friction force. In the non-repeated experiment there is no run-in behavior and the friction force gradually increases with sliding distance. The relative increase in friction is, however, less pronounced in the SiC-on-Si wafer experiment than the sapphire-on-Si wafer experiment. Furthermore, in the repeated SiC experiment, the friction gradually decreases after the run-in phase (up to ~0.4 m sliding, Fig. S1b).

To characterize the wear behavior of the studied interfaces, optical profilometry imaging of the contact region of the balls was performed both before and after the friction experiments (Fig. 2, S4 and S5). The quantitative wear results are given in Table 2, and a summary of all

Table 1
Materials data. The RMS roughness was measured using 5 μm × 5 μm tapping mode AFM measurements at a pixel size of 5 nm.

Material	Type	RMS roughness [nm]
3.18 mm Sapphire ball	Single crystal sapphire	9.0
3 mm SiC ball	Direct sintered SiC	48.7
Si-wafer flat, 0.5 mm thick	Boron doped <100> Si with native oxide layer	0.9
4 mm Glass ball	Soda lime glass (Sigmund Lindner)	36.6
Glass flat, 1 mm thick	Extra white soda lime glass (Thermo scientific)	1.0

predominant wear mechanisms can be found in Table S1. The profilometry images clearly demonstrate that a spherical cap is worn off from the sapphire ball during the non-repeated friction experiment, resulting in an average specific wear rate of $K = 6.5 \pm 2.8 \times 10^3$ μm^3/Nm (based on a minimum of three independent experiments): $K = V/F_nL$ where V is the wear volume, determined based on the profilometry data. The wear scar on the sapphire ball that has undergone repeated sliding looks very different; a substantial amount of compressed debris — or third body [21] — has accumulated on the region of the ball that was in contact with the wafer. This was reproducible for three independent identical experiments. The third body was loosely attached and could easily be removed from the ball surface by cleaning for 60 min in an ultrasonic bath containing acetone (Fig. 2c). Removing the third body revealed that the 'repeated' ball had obviously worn less than in the non-repeated experiment: the average wear rate for the sapphire balls during repeated

Table 2
Wear observations.

Ball	Flat	Sliding mode	$K_{ball} \times 10^3$ [μm^3/Nm]	Third body location	Third body origin
Sapphire	Si wafer	Repeated	1.0 ± 0.4	Predominantly adhered to ball	Si wafer
		Non-repeated	6.5 ± 2.8	Not observed[a]	
SiC	Si wafer	Repeated	9.7 ± 0.5	Predominantly adhered to Si wafer	Si wafer and SiC fragments
		Non-repeated	7.7 ± 1.3	Small amount[b] adhered to ball & Si wafer	

[a] Note that, in a few exceptional cases where the relative humidity of the air environment was slightly higher, a small amount of third body formation was observed on the ball; this was much less than in the repeated case.
[b] Much less than in the repeated case.

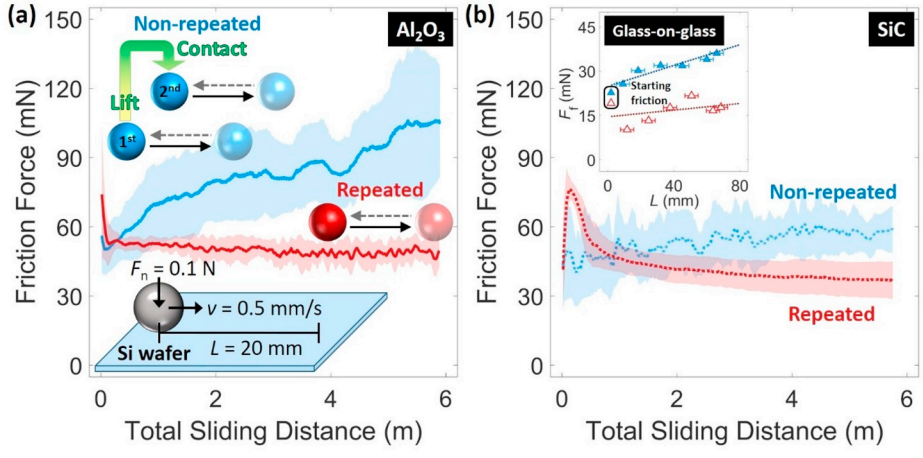

Fig. 1. Friction measurements during repeated and non-repeated sliding of (a) a sapphire ball on a Si wafer and (b) a SiC ball on a Si wafer. Insets in (a) show schematic illustrations of the sliding mode. The inset in (b) shows glass ball on glass flat friction measurements. The solid lines represent the moving average friction force, averaged over 2 cycles, and the shaded areas adjacent to this line indicate the standard deviation in the measured friction forces for a minimum of three identical independent experiments (see also Fig. S3). For the glass-on-glass friction experiments (inset 1b) each data point represents the average friction force for 4 cycles. All three systems display an increase in the friction force (F_f) with sliding distance (L) for non-repeated sliding.

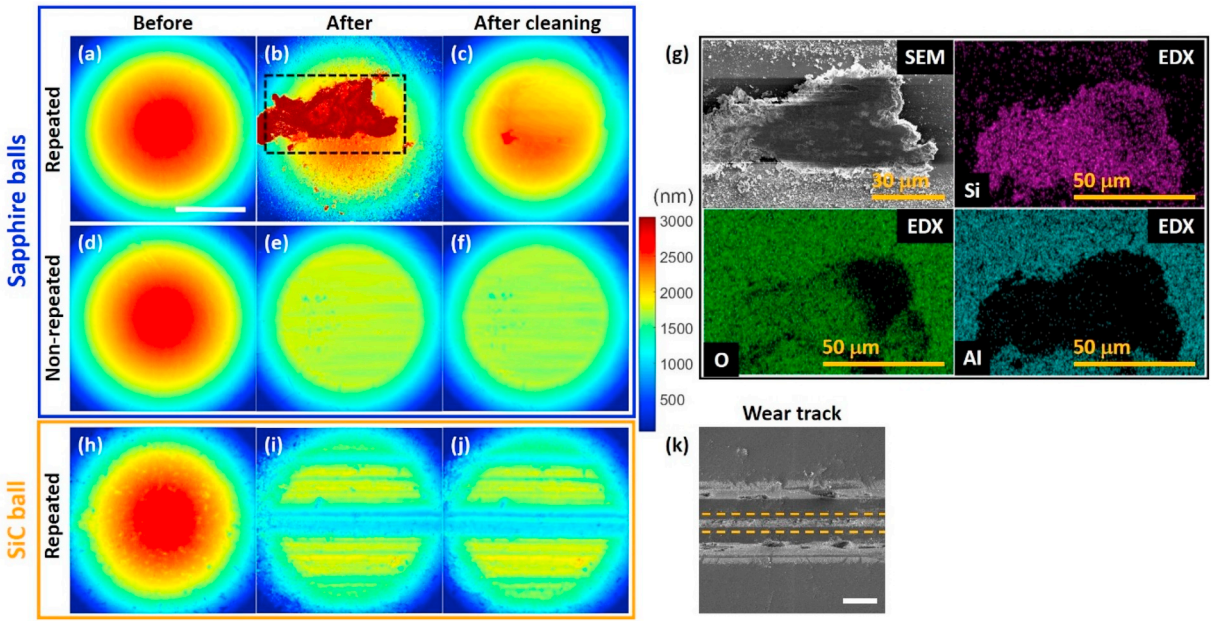

Fig. 2. Ex-situ height profiles and surface characterization of sliding bodies.
(a), (d), (h) Measured height profile before the friction experiment. (b), (e), (i) Measured height profile after the friction experiment. (c), (f), (j) Measured height profile after ultrasonic cleaning of the ball after the friction experiment. (g) SEM and EDX analyses of the third body on the contact zone of the sapphire ball (from b) after a repeated experiment. The silicon (Si) and oxygen (O) signals originate from the third body in the EDX analysis. Little to no aluminum (Al) can be observed within the third body, as compared to the background which consisted of Al_2O_3 (sapphire). (k) SEM image of the wear track and the Si wafer after the repeated SiC experiment (h–j). The orange dashed lines indicate the area within the wear track with increased silicon oxide content. The topography of the wear track matches that of the worn SiC sphere (see also Fig. 3). Scale bars, 50 μm.

sliding was $K = 1.0 \pm 0.4 \times 10^3$ μm^3/Nm: an average of six times less than that measured for the non-repeated experiment.

To understand the nature of the third body formed on the sapphire ball during the repeated experiment, EDX analysis was performed on the ball from Fig. 2b (see Fig. 2g). The measurements indicate that the third body consists mainly of silicon and oxygen and no significant amounts of aluminium, strongly indicating that the third body is wear debris, primarily SiO_x and originating from the Si wafer (Table 2). This is supported by SEM-EDX analysis of the Si flat performed after a repeated experiment, which clearly shows that SiO_x debris particles remain next to the wear track but not inside the wear track (Fig. S6d – f). It is unlikely that the SiO_x originates from accumulation of the native oxide, as the calculated volume of the SiO_x in the contact region on the sapphire ball (Fig. S7) was $\sim 470 \times 10^3$ μm^3, which is much greater than the corresponding approximate volume of native oxide on the Si wafer wear track $(20 \times 10^3 \times 60 \times 2 \times 10^{-3}$ [22] $= 2.4 \times 10^3$ μm^3). More SiO_x debris was observed at the ends and either side the wear track (Fig. S6a, c), than in the central region of the flat. The large amount of debris suggests that an abrasive wear mechanism occurred during sliding. It is unclear whether the silicon wear debris found on the contacts becomes oxidized before, during or after attachment to the ball.

While in the SiC-on-Si wafer experiments the frictional behavior is qualitatively similar to that observed in the sapphire-on-Si wafer experiments, an important difference is that the third body is predominantly located in the central region on the wear track of the Si wafer (Fig. 3b and c) rather than the SiC ball after the repeated sliding experiment (Fig. 2i and j). The third body in this case comprises a ridge of compressed SiO_xC_y debris, likely originating from oxidized Si debris

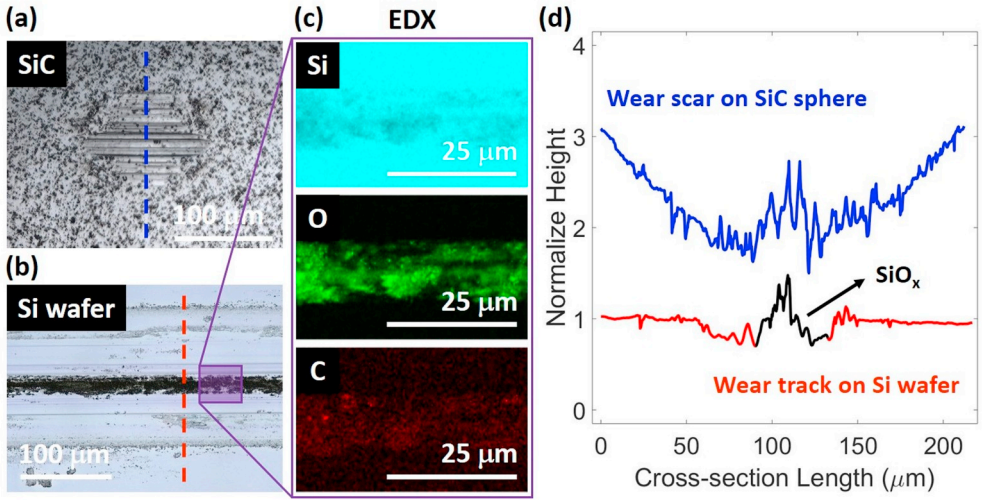

Fig. 3. Surface characterization for the repeated SiC-on-Si wafer experiment.
The optical image of (a) the SiC ball and (b) the corresponding wear track on the Si substrate after a repeated sliding experiment. (c) The EDX analysis demonstrates the formation of SiO_x at the center of the wear track on the wafer, where the results shows less Si signal but a strong O and carbon (C) signal illustrating that C has transferred from the SiC ball to the Si wafer. (d) The height profile taken from the cross-section of (a) and (b) shows that the surface topography of the wear scar and the wear track match, indicating that the sliding motion was likely accommodated at the interface between the ball and the SiO_x.

from the wafer and small fragments of SiC from the ball (Table 2). Furthermore, the profile of this third body, recorded perpendicular to the sliding direction, perfectly matched that observed on the SiC ball (along the same direction, Fig. 3d). This strongly suggests that in the repeated sliding SiC-on-Si wafer experiment, the sliding was accommodated at the ball-on-third body interface. This would then also explain why the difference in ball wear between repeated and non-repeated SiC-on-wafer experiments was much smaller than that in the sapphire-on-Si wafer experiments, in which the SiO_x third body adhered to the ball (in repeated experiments). The SiO_x third body may adhere more strongly to the sapphire ball than to the SiC ball because the sapphire ball was much smoother and therefore more susceptible to physical or capillary adhesion [23]. In all non-repeated experiments, we do not observe such dominant SiO_x third bodies within the wear track on the wafer or on the ball, as seen for repeated experiments.

Our ex-situ observations thus suggest that the observed difference in friction between repeated and non-repeated sliding is related to the formation (or absence) of a third body at the sliding interface. To test this more directly, the friction experiments were repeated, but with different materials, in a microscopy setup (Fig. 4a) consisting of a rheometer mounted on top of an inverted microscope. In this setup, a glass ball is fixed off-center to the rheometer tool which can be rotated

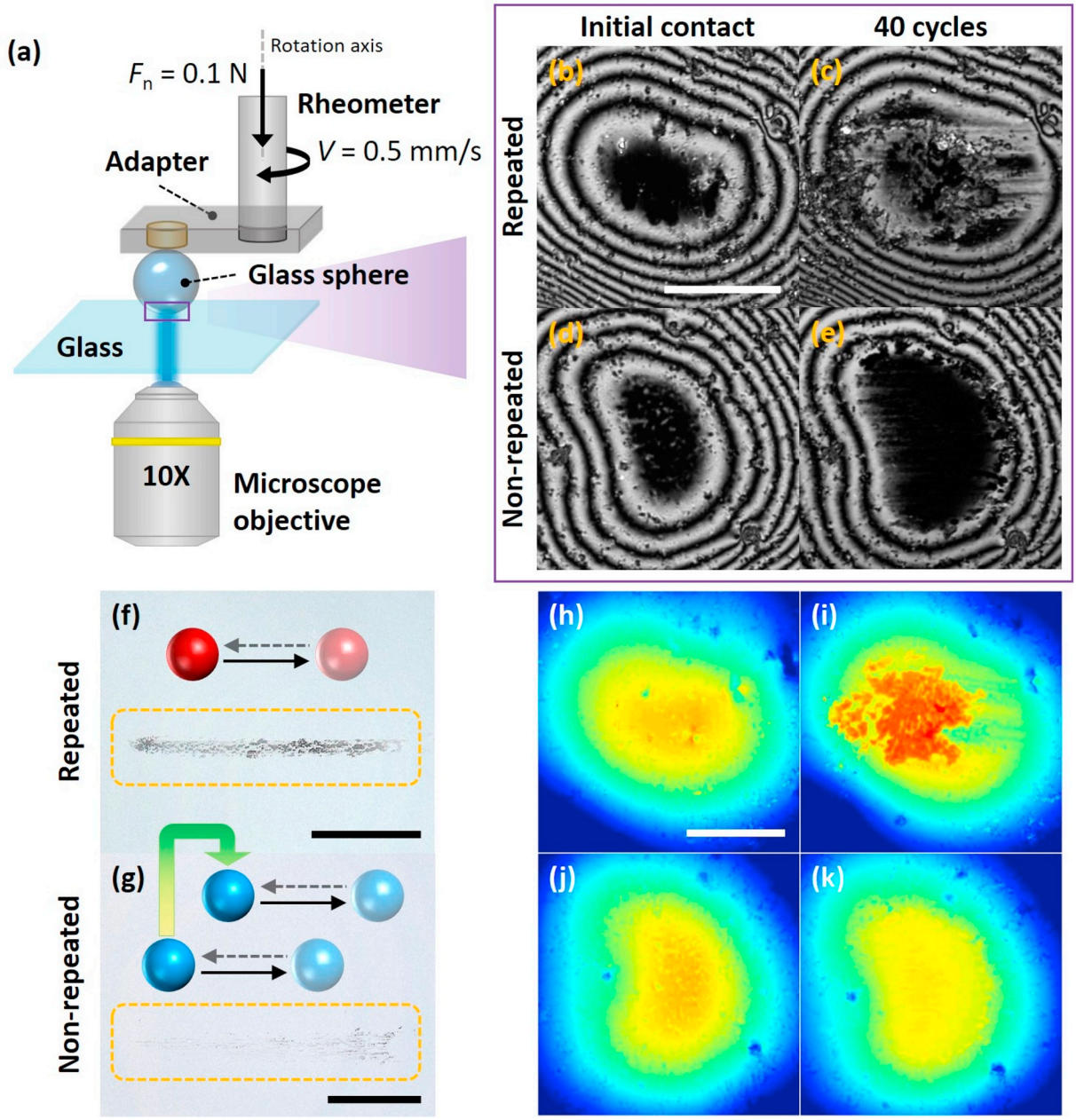

Fig. 4. Imaging of the interface between a glass ball and a float glass coverslip and ex-situ optical images and height profiles recorded before and after the friction experiments.

(a) Visualization/friction experiments were performed using an inverted confocal laser scanning microscope on top of which a rheometer was mounted. The glass ball is fixed to the rheometer tool at a distance of 12.98 mm from the rotation axis. By imposing an angular velocity of 3.52 rad/s, the ball is forced to slide with a velocity of 0.5 mm/s and makes 1 mm strokes. (b), (d) Initial contact at the interface and (h), (j) height profile of glass ball before sliding. Debris is collected at the interface (c) and is observed on the ball (i) and on the substrate (f) after repeated sliding. After non-repeated sliding, there is no visible debris at the interface (e) or on the ball (k), some debris is left on each of the sliding tracks (g). In both experiments the apparent contact area increases as a result of the wear. The contact force is 100 mN in all images. White and black scale bars are 50 μm and 100 μm, respectively. The color scale in (h–k) is identical to that used in Fig. 2.

and moved vertically, enabling measurement of and control over the normal and tangential force exerted at the ball-on-flat interface [24]. As with the UMT experiments, the ball diameter was 4 mm, the normal force was kept at 0.1 N and the sliding speed was 0.5 mm/s. To enable in situ visualization of the interface, the repeated and non-repeated experiments were performed with transparent materials: glass balls on glass flats. The microscope illuminates and images the ball-on-flat interface through the transparent flat. In a typical microscopy image of the interface, we observe a black central region enclosed by interference fringes, the first of which corresponds to a gap of 114.5 nm between the ball and the flat [25]. In the central black region the surfaces have approached to within 114.5 nm, this is the apparent area of contact.

Fig. 4b – e displays the contact images obtained before and after 40 cycles of repeated or non-repeated sliding. Even though the materials are different, it was observed that the glass-on-glass interfaces behave qualitatively similar to the sapphire or SiC-on-Si wafer interfaces studied above: wear debris is collected at the interface as a third body during repeated sliding (Fig. 4c), but not — or much less so — during non-repeated sliding (Fig. 4e). Furthermore, the friction measurements showed that non-repeated sliding results in a clear increase of friction with sliding distance, while repeated sliding does not, or much less so (Fig. 1b inset). Hence we observe that in three different materials systems the friction force measured during a repeated sliding experiment stabilizes after a run-in phase, a phenomenon that has also been observed elsewhere [26], while that measured during non-repeated sliding gradually increases with sliding distance. Based on the microscopy and profilometry measurements (Fig. 4b – k) it can be concluded that, during the run-in phase observed in repeated experiments, debris particles were compressed into a third body that subsequently stabilizes the friction: supplementary Movies S1 – S3 show a typical example of the glass-on-glass interface recorded during repeated sliding (S1), non-repeated sliding (S2) and lifting of the sphere (S3) after repeated sliding. It is important to note that while non-repeated sliding suppresses the formation of a third body, we still observed a third body in some non-repeated sapphire-on-Si wafer experiments that were carried out in an air environment with a slightly higher average relative humidity of 45%, compared to other experiments at 34%. For these particular experiments, the friction measurements showed run-in behavior similar to that in the repeated experiments (Fig. S2). As mentioned previously, the exceptionally low roughness of the sapphire balls (Fig. 5 and S8) may enable wear debris to adhere to the ball surface through capillary or physical adhesion, even in some of the non-repeated experiments.

Supplementary video related to this article can be found at https://doi.org/10.1016/j.triboint.2019.105983.

Our results thus show that there is much less chance of third body formation at the interface during non-repeated sliding. In this case, it is important to consider the mechanism responsible for the gradual increase in friction observed in such experiments (e.g. Fig. 1). To address this question, the wear behavior for sapphire-on-Si wafer interfaces was analyzed in more detail.

The effect of the wear should be considered in terms of the continuous change in the real contact pressure and real area of contact occurring at the sliding interface during the wear process, which is difficult to determine experimentally. Ignoring roughness, the change in contact pressure between the start and end of the experiment can be estimated by calculating the Hertzian contact stress (P_{Hertz}) at the start and, assuming a fully conforming contact, the contact pressure at the end of the experiment (P_{final}). This gives a change in contact pressure from $P_{Hertz} = 428$ MPa to $P_{final} = 11.4$ MPa, where the latter value is based on the area of the flat cap worn off of the ball in Fig. 5c. Note that the real contact pressure at the start of the experiment is likely to be higher than P_{Hertz} because the ball and wafer roughness is not taken into account. To estimate the effect of roughness, we carry out boundary element model (BEM) calculations [27], which in this case were performed using the Tribology Simulator that is publicly available at

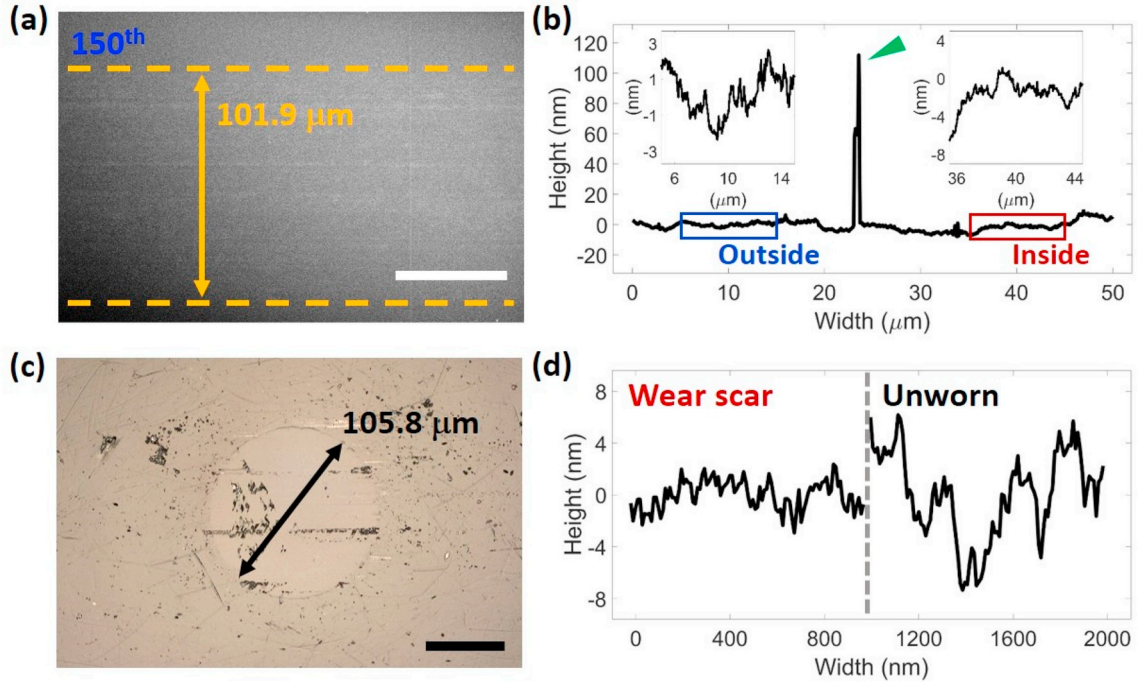

Fig. 5. The surface topography before and after a non-repeated sapphire-on-Si wafer experiment.
(a) SEM image of the last (150^{th}) wear track on the wafer. (b) AFM line scan of the last wear track on the wafer recorded perpendicular to the sliding direction. The green arrow indicates the edge of the wear track at which debris particles were occasionally found. Inset figures show the surface roughness outside and inside the wear track. (c) Microscopy image of the sapphire ball. The width of the wear scar on the ball matches that of the track on the wafer (a). (d) AFM line profiles measured in- and outside the wear scar on the sapphire ball. The roughness of the wear scar ($R_q = 2.6 \pm 0.9$ nm) is significantly smaller than that measured on the unworn sapphire ($R_q = 9.0 \pm 3.3$ nm). Scale bars, 50 μm.

Tribonet [28] and using data from optical profilometry of the ball before and after the sliding experiment. These simulation results are limited by the resolution and quality of the optical profilometry measurements, which were carried out with a resolution of approximately 50 nm in lateral and 20 nm in height directions. The results of the calculated contact gap profiles are shown in the supplementary information Figs. S9a and S9b and yield real contact pressures of 2.62 GPa and 0.35 GPa for, respectively, the initial contact and after sliding. Although, as expected, these surface pressures are much higher than those calculated without roughness, it is evident that a large decrease in contact pressure occurs. Thus, the real contact pressure and real contact area rapidly change as a result of wear, and the wear rate is unlikely to be constant.

A different way to consider the wear behavior is to estimate the rate of material removal on the atomic scale. For rough surfaces, the maximum contact pressure exerted at the sapphire-on-Si-wafer interface can never exceed the hardness of the Si-wafer: this would cause the wafer to plastically deform such that the area of real contact increases and the contact pressure drops below the hardness again. This means that during the (non-repeated) sapphire-on-Si wafer friction experiments the *minimum* area of real contact (A_{min}) between the ball and the substrate is:

$$A_{min} = \frac{F_n}{H} \tag{1}$$

where $F_n = 0.1$ N and $H = 5.1$ GPa is the hardness of the boron doped single crystal silicon <100> wafer that we used [29], yielding:

$$A_{min} = 2 \times 10^{-11}\ \text{m}^2 \approx \frac{2 \times 10^{-11}}{(2 \times 10^{-10})^2} = 5 \times 10^8\ \textit{atoms} \tag{2}$$

Thus, over the whole area of the contact, at least 5×10^8 *atoms* on the ball surface must touch and slide over the wafer surface at any time, where 2×10^{-10} m is used as an approximate atom-to-atom distance within the ball (note that the goal of this calculation is to provide only order-of-magnitude estimates). Using as an example the total wear volume of the sapphire ball shown in Fig. 5c, measured after a sliding distance of 6 m, we can estimate how many atoms on the ball surface are worn off during a non-repeated experiment:

$$\frac{3.9 \times 10^{-15}\ \text{m}^3}{(2 \times 10^{-10}\ \text{m})^3} \approx 5 \times 10^{14}\ \textit{atoms} \tag{3}$$

It follows that on average, atoms on the ball surface that make contact with the substrate slide at least 6 μm before they are worn off:

$$\frac{6\ \text{m} \times 5 \times 10^8}{5 \times 10^{14}} = 6\ \mu\text{m} \tag{4}$$

We therefore conclude that the ball wear is very mild and the above analysis suggests that this may even occur atom-by-atom [30,31]: when the ball slides over a distance that is the equivalent of more than tens of thousands of atomic spacings, only a single atomic layer is worn off from the sapphire ball.

The wear tracks that are left on the silicon wafer after the non-repeated experiment were also analyzed using AFM and SEM imaging. Although the very first strokes on the wafer may involve some abrasive wear resulting in scratches on the wafer, no, or very little, evidence of wear was found during the subsequent strokes (Figs. 5a and 6b); the wafer roughness is greater than the height difference measured inside and outside the tracks (Fig. 5b).

These observations and calculations suggest that adhesive friction, controlled by the area of real contact, is the main friction mechanism in the non-repeated experiment. The wear may however be governed by the tribochemical behavior at the interface [32]. An adhesion friction mechanism is also supported by the observation that for pristine sapphire-on-Si wafer interfaces the friction force — measured at varying normal forces during 100 μm strokes — is strictly proportional to the normal force (Fig. 6a), despite the fact that the apparent area of contact does not increase linearly with the normal force for ball-on-flat interfaces [33]. To further study the interplay between this coefficient of friction and the wear that occurs in non-repeated experiments, a sapphire ball was subjected to a milling procedure. The ball was worn by sliding it along a 6 m spiral-shaped track over the wafer at a fixed normal force of 50 mN. This spiral-shaped sliding track ensured that the ball always encountered fresh wafer surface during the whole experiment. Based on the observations above, it is reasonable to assume that this type of sliding avoids the build-up of a third body on the sphere; indeed AFM PeakForce Tapping measurements [34] performed after the milling procedure confirm this (Fig. S10). Repetition of the non-repeated friction experiment after the ball had been worn in this way showed that the coefficient of friction had substantially increased (Fig. 6a), similar to the behavior observed in the non-repeated sapphire-on-Si wafer experiments (Fig. 1a). Interestingly, if the surrounding air is replaced with dry nitrogen (N_2), a lower coefficient of friction of $\mu = 0.57$ was measured, a value between that measured before wearing the ball ($\mu = 0.50$) and after milling ($\mu = 0.65$) in ambient conditions.

These experiments can be interpreted as follows: During the milling procedure, and also during non-repeated sliding, the surface roughness on the balls is reduced as a consequence of mild wear (Fig. 5). This reduced roughness leads to a larger area of real contact and with that a greater adhesive friction and friction coefficient [35]. Additionally, as

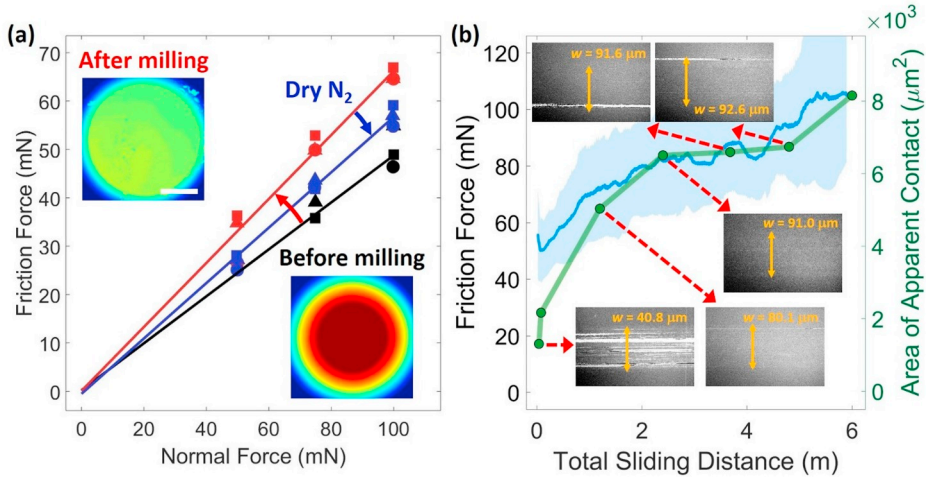

Fig. 6. The friction at a sapphire-on-Si wafer interface.
(a) Friction measurements at varying normal forces were performed in a non-repeated fashion using 100 μm (unidirectional) strokes and a sliding speed of 50 μm/s (black data points). The coefficient of friction increases substantially (red data points) after the ball has been worn (see main text). The coefficient of friction is lower when measured in dry N_2 (blue data points, measured after milling) compared to the ambient measurement. The inset figures show the height profile of the sapphire ball before and after the friction experiments. The color scale is identical to that used in Fig. 2. Scale bar, 50 μm. (b) The area of apparent contact (A_p) between a sapphire ball and a Si wafer is calculated using the width (w) of the wear tracks on the wafer: $A_p = \pi \times w^2/4$. Inset, SEM images of the various wear tracks.

the ball becomes smoother, the total area, within which the gap between the ball and the flat is only a few nanometers, becomes larger (Fig. 5d). Across such nanometric gaps, the water layers that cover most surfaces in ambient conditions can form capillary bridges [36–38], thereby pulling the surfaces into closer contact and increasing the friction [39]. This capillary effect can however be reversed by changing the atmosphere at the interface to dry N_2, thereby removing the influence of the capillary bridges (Fig. 6a). Furthermore, since the capillary effect is active at locations across the interface with a finite gap, the friction can be expected to correlate with the apparent area of contact: the larger the apparent area of contact, the larger the area within which the contacting surfaces experience adhesion: adhesion becomes significant and dominates the friction force when there is high surface conformity and the average gap between the contacting surfaces, defined as the sum of the RMS roughness of the two surfaces, is less than 10 nm [40]. This is indeed observed; by analyzing the wear tracks on the Si wafer, the apparent area of contact was measured at various stages during the non-repeated sapphire-on-Si wafer experiment. The result is plotted in Fig. 6b alongside the friction measurements in ambient conditions to show that the gradual growth of the apparent area of contact closely tracks that of the friction force.

4. Summary and closing remarks

Summarizing, the difference between repeated and non-repeated sliding has been studied systematically for various interfaces between non-metallic brittle materials in ambient air conditions. It has been demonstrated that the sliding mode is a very important parameter: Identical systems were shown to give widely varying friction and wear behavior depending on whether the sliding is repeated or non-repeated; for sapphire-on-Si wafer contacts the sapphire wear changed by a factor 6 and the friction force varied by a factor 2. In the case of SiC-on-Si wafer, the increase in friction observed during a non-repeated experiment was smaller. It is hypothesized that this difference between sapphire and SiC may be explained by the grain structure of the sintered SiC balls, which is not present in the single crystal sapphire balls; such grain structure may enable the SiC balls to maintain a minimum level of roughness that is larger than that of the wafer. Indeed, the worn SiC surfaces are rougher than the worn sapphire surfaces (Fig. S8). An additional important difference between the sapphire and SiC experiments is that, in repeated experiments, the SiO_x third body forms on the ball when a sapphire ball is used but within the Si-wafer wear track when a SiC ball is used, indicating that the wear debris adheres more readily to sapphire than SiC. This difference between sapphire and SiC may again be caused by the surface roughness; since the sapphire surface is smoother than the SiC surface, debris may adhere more readily to the sapphire through physical or capillary adhesion. In fact, we observe that even in some of the non-repeated sapphire-on-Si wafer experiments wear debris can adhere to the sapphire surface (Fig. S2). Indeed those experiments in which we observed this third body formation and the associated run-in behavior, were performed at a slightly higher relative humidity compared to the otherwise identical experiments in which we did not observe run-in. If capillary adhesion is responsible for the sticking of the wear debris, this correlation could be expected. However, further research is clearly needed in order to investigate and fully explain this phenomenon. The sliding distance required to achieve stable friction in the repeated experiments was also longer for SiC than for sapphire. This difference may be a consequence of the fact that in the SiC experiment, the SiO_x third body needs to form over the entire 20 mm sliding track on the wafer, while in the sapphire experiment it is sufficient to form this SiO_x body only on top of the ball. Furthermore, because in this SiC experiment the third body is immobilized on the wafer rather than on the ball, the ball can be expected to wear more, as observed (Fig. 2i). It has thus been shown that while repeated sliding steers all systems toward the formation of a third body that stabilizes the friction — which was observed in situ for glass-on-glass interfaces — in non-repeated sliding no evidence for such third body formation is found. In all the studied systems, non-repeated sliding leads to a gradual increase of the friction coefficient with sliding distance. Based on an in-depth analysis of the sapphire-on-Si wafer system, including wear calculations, AFM, contact pressure calculations and dedicated wear experiments, it is proposed here that the mechanism behind the increase in friction with sliding distance is a gradual loss of slider surface roughness that not only increases the (nominally dry) area of real contact, but also leads to more capillary bridges across the interface and potentially allows van der Waals forces to become significant by decreasing the average gap between the surfaces; all of these effects result in higher friction. This interplay between surface roughness, capillarity and the area of real contact is complex, but likely universal since virtually all surfaces are rough and covered by water layers.

Acknowledgements

This work has been carried out at the Advanced Research Center for Nanolithography (ARCNL), a public-private partnership of the University of Amsterdam (UvA), the Netherlands, the Vrije University Amsterdam (VU), the Netherlands, the Dutch Research Council (NWO) and the semiconductor equipment manufacturer ASML. The authors would like to thank Camila Blanco Bilbao (University of Sheffield, UK), Zazo Meijs and Arend-Jan van Calcar (ARCNL) for their technical assistance.

Appendix A. Supplementary data

Supplementary data to this article can be found online at https://doi.org/10.1016/j.triboint.2019.105983.

References

[1] Holmberg K, Erdemir A. Global impact of friction on energy consumption, economy and environment. FME Trans 2015;43:181–5.
[2] Holmberg K, Erdemir A. Influence of tribology on global energy consumption, costs and emissions. Friction 2017;5:263–84.
[3] Grabon W, Koszela W, Pawlus P, Ochwat S. Improving tribological behaviour of piston ring–cylinder liner frictional pair by liner surface texturing. Tribol Int 2013;61:102–8.
[4] Greco A, Sheng S, Keller J, Erdemir A. Material wear and fatigue in wind turbine Systems. Wear 2013;302:1583–91.
[5] Tyfour WR, Beynon JH, Kapoor A. The steady state wear behaviour of pearlitic rail steel under dry rolling-sliding contact conditions. Wear 1995;180:79–89.
[6] Tremblay MR, Cutkosky MR. Estimating friction using incipient slip sensing during a manipulation task. In: Proc. IEEE int. Conf. Robot. Autom., IEEE Comput. Soc. Press. vol. 2002; 1993. p. 429–34.
[7] Luck DL, de Boer MP, Ashurst WR, Baker MS. Evidence for pre-sliding tangential deflections in MEMS friction. In: TRANSDUCERS '03. 12th int. Conf. Solid-state sensors, Actuators microsystems. Dig. Tech. Pap. (Cat. No.03TH8664). vol. 1; 2003. p. 404–7. IEEE.
[8] Gallardo-Hernandez EA, Lewis R. Twin disc assessment of wheel/rail adhesion. Wear 2008;265:1309–16.
[9] Grönqvist R. Mechanisms of friction and assessment of slip resistance of new and used footwear soles on contaminated floors. Ergonomics 1995;38:224–41.
[10] Dahiya RS, Metta G, Valle M, Sandini G. Tactile sensing—from humans to humanoids. IEEE Trans Robot 2010;26:1–20.
[11] Bonnet C, Valiorgue F, Rech J, Claudin C, Hamdi H, Bergheau JM, et al. Identification of a friction model—application to the context of dry cutting of an AISI 316L austenitic stainless steel with a TiN coated carbide tool. Int J Mach Tool Manuf 2008;48:1211–23.
[12] Khurshudov A, Waltman RJ. Tribology challenges of modern magnetic hard disk drives. Wear 2001;251:1124–32.
[13] Celano U, Hsia F-C, Vanhaeren D, Paredis K, Nordling TEM, Buijnsters JG, et al. Mesoscopic physical removal of material using sliding nano-diamond contacts. Sci Rep 2018;8:2994.
[14] Gosvami NN, Bares JA, Mangolini F, Konicek AR, Yablon DG, Carpick RW. Mechanisms of antiwear tribofilm growth revealed in situ by single-asperity sliding contacts. Science 2015;348:102–6.
[15] Laux KA, Schwartz CJ. Influence of linear reciprocating and multi-directional sliding on PEEK wear performance and transfer film formation. Wear 2013;301:727–34.
[16] Ward R. A comparison of reciprocating and continuous sliding wear. Wear 1970;15:423–34.

[17] Odabaş D, Su Ş. A comparison of the reciprocating and continuous two-body abrasive wear behavior of solution-treated and age-hardened 2014 Al alloy. Wear 1997;208:25–35.
[18] Singer IL, Dvorak SD, Wahl KJ, Scharf TW. Role of third bodies in friction and wear of protective coatings. J Vac Sci Technol A Vacuum, Surfaces, Film 2003;21: S232–40.
[19] Kim I-J, Smith R, Nagata H. Microscopic observations of the progressive wear on shoe surfaces that affect the slip resistance characteristics. Int J Ind Ergon 2001;28: 17–29.
[20] Poiesz T, Achanta S, Akbas, Mehmet A, Antonov P, Bouwknegt J, et al. A substrate holder and a method of manufacturing a substrate holder. WO/2018/007498. 2018.
[21] Deng F, Tsekenis G, Rubinstein SM. Simple law for third-body friction. Phys Rev Lett 2019;122:135503.
[22] Kahn H, Deeb C, Chasiotis I, Heuer AH. Anodic oxidation during MEMS processing of silicon and polysilicon: native oxides can be thicker than you think. J Microelectromechanical Syst 2005;14:914–23.
[23] Pastewka L, Robbins MO. Contact between rough surfaces and a criterion for macroscopic adhesion. Proc Natl Acad Sci 2014;111:3298–303.
[24] Weber B, Suhina T, Junge T, Pastewka L, Brouwer AM, Bonn D. Molecular probes reveal deviations from Amontons' law in multi-asperity frictional contacts. Nat Commun 2018;9:888.
[25] Jenkins Francis A, White HE. Fundamentals of optics. fourth ed. New York: Tata McGraw-Hill Education; 1976.
[26] Chen L, Kim SH, Wang X, Qian L. Running-in process of Si-SiO x/SiO2 pair at nanoscale—sharp drops in friction and wear rate during initial cycles. Friction 2013;1:81–91.
[27] Müser MH, Dapp WB, Bugnicourt R, Sainsot P, Lesaffre N, Lubrecht TA, et al. Meeting the contact-mechanics challenge. Tribol Lett 2017;65:118.
[28] Tribonet. https://www.tribonet.org.
[29] Bhushan B, Li X. Micromechanical and tribological characterization of doped single-crystal silicon and polysilicon films for microelectromechanical systems devices. J Mater Res 1997;12:54–63.
[30] Jacobs TDB, Carpick RW. Nanoscale wear as a stress-assisted chemical reaction. Nat Nanotechnol 2013;8:108–12.
[31] Liu J, Jiang Y, Grierson DS, Sridharan K, Shao Y, Jacobs TDBB, et al. Tribochemical wear of diamond-like carbon-coated atomic force microscope tips. ACS Appl Mater Interfaces 2017;9:35341–8.
[32] Chen L, Wen J, Zhang P, Yu B, Chen C, Ma T, et al. Nanomanufacturing of silicon surface with a single atomic layer precision via mechanochemical reactions. Nat Commun 2018;9:1542.
[33] Suhina T, Weber B, Carpentier CE, Lorincz K, Schall P, Bonn D, et al. Fluorescence microscopy visualization of contacts between objects. Angew Chem Int Ed 2015; 54:3688–91.
[34] Fischer H, Stadler H, Erina N. Quantitative temperature-depending mapping of mechanical properties of bitumen at the nanoscale using the AFM operated with PeakForce Tapping TM mode. J Microsc 2013;250:210–7.
[35] Weber B, Suhina T, Brouwer AM, Bonn D. Frictional weakening of slip interfaces. Sci Adv 2019;5:eaav7603.
[36] Asay DB, Kim SH. Evolution of the adsorbed water layer structure on silicon oxide at room temperature. J Phys Chem B 2005;109:16760–3.
[37] Hasz K, Ye Z, Martini A, Carpick RW. Experiments and simulations of the humidity dependence of friction between nanoasperities and graphite: the role of interfacial contact quality. Phys Rev Mater 2018;2:126001.
[38] Chen L, Xiao C, Yu B, Kim SH, Qian L. What governs friction of silicon oxide in humid environment: contact area between solids, water meniscus around the contact, or water layer structure? Langmuir 2017;33:9673–9.
[39] Bazrafshan M, de Rooij MBB, Schipper DJJ. Adhesive force model at a rough interface in the presence of thin water films: the role of relative humidity. Int J Mech Sci 2018;140:471–85.
[40] Delrio FW, de Boer MP, Knapp JA, David Reedy E, Clews PJ, Dunn ML, et al. The role of van der Waals forces in adhesion of micromachined surfaces. Nat Mater 2005;4:629–34.